Dynamic network modeling of two-phase drainage in porous media

Mohammed S. Al-Gharbi and Martin J. Blunt
Department of Earth Science and Engineering, Imperial College, London SW7 2AZ, United Kingdom
(Received 21 January 2004; published 13 January 2005)

We present a dynamic network model for modeling two-phase flow. We account for wetting layer flow, meniscus oscillation, and the dynamics of snapoff. Interfaces are tracked through pore elements using a modified Poiseuille equation for the equivalent hydraulic resistance of the fluids between the pore element centers. The model is used to investigate the effects of capillary number and viscosity ratio on displacement patterns and fractional flow in primary drainage. We show that the amount of snapoff increases with increasing capillary number and decreasing wetting phase viscosity. For capillary numbers lower than approximately 10^{-5}, the pore-scale fluid distribution and fractional flow are similar to those obtained using a quasistatic model that ignores viscous forces. The contribution of oil transport from ganglia, formed by snapoff, is negligible except for very large capillary numbers, greater than around 0.1.

DOI: 10.1103/PhysRevE.71.016308 PACS number(s): 47.55.Mh, 47.55.Dz, 47.55.Kf

I. INTRODUCTION

Understanding multiphase flow in porous media is important for a number of practical applications, including the implementation of improved recovery schemes from hydrocarbon reservoirs, contaminant cleanup, and designing underground nuclear waste repositories. Fundamentally, the geometry of the void space of a porous medium and the interactions of the multiple phases with the solid determine macroscopic properties such as porosity, relative permeability, capillary pressure, and resistivity index [1,2]. One approach to predicting these quantities is through pore-scale modeling that requires a detailed understanding of the physical processes occurring at the pore scale and a complete description of the morphology of the pore space.

The pore-scale network is a representation of the void space of the reservoir rock. Wide void spaces are represented by pores that are connected by narrower regions called throats. Then using rules for determining fluid configurations and appropriate flow and transport equations, multiphase flow is computed in the network. An excellent description of different types of pore-scale network models can be found in the classic text by Dullien [2], while more recent reviews are to be found in Refs. [3,4].

The majority of the existing pore network models are quasistatic [1,4–11] assuming that capillary forces alone control the fluid configuration in the pore space: capillary pressure is imposed on the network and the final, static position of all fluid-fluid interfaces is determined, ignoring the dynamic aspects of pressure propagation and interface dynamics due to viscous forces.

There are many important circumstances where the assumption of purely capillary-controlled displacement at the pore scale is not appropriate. The ratio of viscous to capillary pressure is conventionally defined using a capillary number Ca [2],

$$\mathrm{Ca} = \frac{\mu q}{\sigma}, \tag{1}$$

where μ is the viscosity of the displacing phase, q is the total Darcy velocity (volume flowing per unit area per unit time), and σ is the interfacial tension between the two fluid phases. For typical oil/water flows in reservoirs, μ is around 10^{-3} Pa s, σ is 0.05 N m^{-1}, and q is 10^{-5} ms^{-1} or lower, giving $\mathrm{Ca} \simeq 2 \times 10^{-7}$. Viscous forces become significant at the pore scale only when Ca is the range 10^{-4}–10^{-3} or larger [2]. Hence quasistatic models are often accurate and can predict a variety of low-flow-rate experiments successfully [1,4]. However, if the viscosity is high (polymer flooding), the flow rate is very large (for instance, in fractures, gas reservoirs, and near well bores) or the interfacial tension is low (surfactant flooding, near-miscible gas injection, and gas condensate reservoirs), viscous and capillary forces can be comparable at the pore scale. In these cases, a number of effects, such as the movement of disconnected ganglia of oil and the simultaneous filling of neighboring pores become significant [12].

Dynamic network models explicitly account for viscous forces: a specified inflow rate for one of the fluids is imposed and the subsequent transient pressure response and the associated interface positions are calculated. Koplik and Lasseter [13] simulated primary drainage in networks of spherical pores connected to cylindrical pore throats. Toubou *et al.* [14] and Blunt *et al.* [15] used a simplification of the model of Koplik, assuming that the pores have volume but no resistance to flow and the throats have resistance to flow but no volume. Payatakes and co-workers [16–20] simulated flow in a network of spherical chambers connected through long cylindrical throats with a sinusoidally varying cross section. We will use a similar geometry in our work. They concluded that a significant fraction of the oil flow even at reservoir rates is accommodated through the movement of disconnected ganglia. Celia and co-workers [21–24] extended the model of Blunt *et al.* [15] to study the effect of material heterogeneities on the capillary pressure-saturation relationship [21], effect of nonzero stress at the fluid-fluid interface [22], interfacial area and its relation to capillary pressure [23], and interfacial velocity [24]. Recently Hansen and co-workers [25–27] developed a dynamic network to study fluid movement in drainage and imbibition. They used a network of tubes that connected to each other through volumeless nodes.

The capillary pressure within the tube was a function of the location of the interface.

All these previously developed models except [19] only allowed a single phase to be present in any cross section through a throat—that is, they ignored contributions to flow through wetting layers that occupy the roughness and crevices of the pore space even when the center of the pore or throat is filled by a nonwetting phase [4]. Blunt Scher [28] and Hughes and Blunt [29] did accommodate wetting layer flow in a perturbative model where the wetting layers were all assigned a fixed conductance and where simultaneous filling of multiple pores was disallowed. They showed that rate effects can have a significant effect on the trapping of the nonwetting phase (oil) during imbibition for capillary numbers as low as 10^{-6}, since the ratio of the viscous to capillary force can be high, even at low flow rates, if flow occurs through low conductivity layers. Mogensen and Stenby [30] also assumed a fixed conductance to the wetting layers in their dynamic model of imbibition. They concluded that the capillary number, aspect ratio (ratio of average pore diameter to average throat diameter), and contact angle all have a significant influence on the competition between pistonlike advance (frontal movement of a phase displacing another in a throat) and snapoff (where wetting phase flows through layers and fills narrow regions of the pore space in advance of a connected front). Singh and Mohanty [31] developed a dynamic model to simulate two-phase flow. They used a cubic network with cubic pores and throats of square cross section. A pseudopercolation model was included in the model for simulating low capillary number flow. In their model, the volume flowing in the wetting layers was set to be 1% of the volume flowing through the bulk. The model was used to study primary drainage with constant inlet flow rate. Saturation and relative permeability were computed as a function of capillary number, viscosity ratio, and pore-throat size distribution.

Despite this extensive literature on dynamic pore-scale modeling, a number of key physical effects have yet to be captured accurately. In particular, previous work did not account for the swelling of wetting layers in both drainage and imbibition that allows snapoff, as observed in micromodel experiments [14]. Snapoff is the key process by which the nonwetting phase becomes trapped, and determines, for instance, the amount of oil that is left unrecovered after water flooding. Related to this lack of physical realism is a controversy in the literature over the generic nature of multiphase flow in porous media. The conventional picture, based largely on quasistatic approaches to modeling, assumes that for typical reservoir displacements each phase occupies its own connected subnetwork through the porous medium. The hydraulic conductance of these subnetworks determine the multiphase flow properties, specifically the relative permeability [2,4]. Disconnected regions do not flow unless the capillary number is very high. In contrast, Payatakes *et al.* [16–20] suggest based on micromodel experiments and network modeling that the typical scenario for multiphase flow is significant transport via disconnected ganglia even at reservoir flow rates. However, some of their work can be criticized for not accommodating wetting layer flow and consequently substantially restricting the connectivity of the wetting phase.

In this work we introduce a conceptually simple dynamic model that explicitly simulates the dynamics of wetting layer swelling and snapoff. We are then able to address whether or not multiphase flow involves significant transport of the disconnected nonwetting phase, even at typical reservoir flow rates, or whether this phenomenon is restricted to high capillary numbers.

II. PRINCIPLES OF THE MODEL

The model is based on three main principles.

(1) The amount of each phase in each pore or throat is known at each time step. The volume of each phase (with the contact angle) controls the configuration of fluids. This in turn determines the curvature of the oil-water interface and the pressure difference between these two fluids in each pore or throat.

(2) By using equivalent networks of electrical resistors, the hydraulic resistances of the fluids between pore and throat centers are calculated and used in a volume balance equation to obtain the fluid pressures at pore and throat centers. Using an equivalent resistor network simplifies the problem and makes it no more complex than solving the material balance equations for single-phase flow.

(3) The pressure difference between the pore and throat centers and the previously computed hydraulic resistances of each phase are used to move phases between pores and throats and hence to update the fluid volumes. The simulation then returns to step (1).

III. NETWORK AND PORE GEOMETRY

The porous medium is represented by a square lattice of pores and throats. In cross section each pore or throat is a scalene triangle. The inscribed radius of a pore or throat varies sinusoidally, as shown in Fig. 1 [9]. Each pore is divided into several branches (equal to the number of connected throats), which are considered as extensions of the throats they are connected to. All the pore branches meet at the center of the pore that is treated as a volumeless joining point. This feature is introduced for two reasons. First, we believe it is more realistic than assuming a straight channel (i.e., uniform inscribed radius along the length). Second, it allows us to assign a unique and continuously varying capillary pressure as the interface (meniscus) moves in a pore or throat. The inscribed radius (R) at any point between the pore and the connecting throat centers is given by

$$R = \left(\frac{R_p + R_t}{2}\right) + \left(\frac{R_p - R_t}{2}\right)\cos\left(\frac{2\pi x}{l_p + l_t}\right), \tag{2}$$

where R_p and R_t are the pore and throat center radii, respectively, l_p and l_t are the pore and throat lengths, respectively. $x=0$ at the pore center and $x=(l_p+l_t)/2$ at the throat center.

A. Selection of pore and throat sizes

The inscribed radius of the center of any throat is assigned at random according to a truncated Weibull distribution

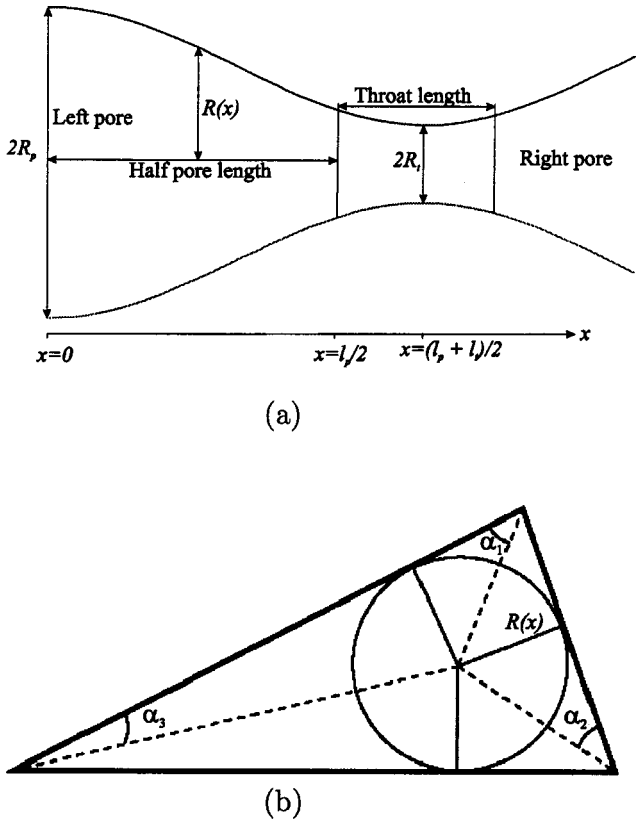

FIG. 1. Schematic diagram of pore and throat geometries. (a) Side view: the inscribed radius of the pore element varies sinusoidally with the length. (b) Cross-sectional view: the pore element has a triangular cross section. α is the corner half angle.

$$R_t = (R_{t,max} - R_{t,min})\{-\delta \ln[z(1-e^{-1/\delta}) + e^{-1/\delta}]\}^{1/\varrho} + R_{t,min}, \tag{3}$$

where R_t is a radius of a throat center and z is a random number between 0 and 1. The parameters used in the distribution are shown in Table I. The pore radius at its center must be greater or equal to the maximum radius of the connecting throats. Therefore the pore radius is given by the following expression:

TABLE I. Parameters used to determine pore and throat geometries.

Parameter	Value
$R_{t,min}$	0.2 μm
$R_{t,max}$	100 μm
l_{min}	1 μm
l_{max}	50 μm
a_{max}	2.2
a_{min}	2.0
δ	0.8
ϱ	1.6

$$R_p = \max\{R_{ti} | i = 1, \ldots, n\}a, \tag{4}$$

where n is the number of the connecting throats, and the aspect ratio (a) is the ratio between the pore radius and the maximum radius of the connecting throats. The aspect ratio is obtained by using Eq. (3), replacing $R_{t,max}$ and $R_{t,min}$ by the maximum and minimum aspect ratios provided in Table I. While we use a topologically square lattice, we do allow the pore and throat lengths to vary—this corresponds physically to a distorted lattice, although we do not check if the network is physically realizable in two-dimensional space. We used the same parameters for selecting the pore and throat lengths, replacing $R_{t,max}$ and $R_{t,min}$ by l_{max} and l_{min} provided in Table I in Eq. (3). Once l_p, l_t, R_p, and R_t are known, Eq. (2) is used to determine the inscribed radius as a function of distance between the pore and throat centers.

B. Determination of the pore cross section and corner half angles

Each pore and throat has a scalene triangular cross section with corner angles selected at random. The triangular cross section of an element is determined through two parameters: the inscribed radius (described above), and the shape factor $F=A/P^2$, where A is the cross sectional area and P is the perimeter [32]. The shape factor is used to determine the corner half angles for a triangle. In our model, we assume that the shape factor for each pore and throat is chosen according to the truncated Weibull distribution [Eq. (3)] for a range of shape factor between zero and $\sqrt{3}/36$ (equilateral),

$$F = \frac{A}{P^2} = \frac{1}{4\sum_{i=1}^{3} \cot(\alpha_i)} = \frac{1}{4}\tan\,\alpha_1 \tan\,\alpha_2 \cot(\alpha_1 + \alpha_2), \tag{5}$$

where α_1 and α_2 are the two corner half angles subtended at the longest sides of the triangle. It is clear from the above equation that for a single value of the shape factor, there are ranges of corner half angles and triangular shapes. We follow the procedure of Patzek [10] to select a nonunique solution for corner half angles.

(1) Select the upper and lower limits of the second largest corner half-angle. These two limits are given according to the following equations

$$\alpha_{2,min} = \arctan\left[\frac{2}{\sqrt{3}}\cos\left(\frac{\arccos(-12\sqrt{3}F)}{3} + \frac{4\pi}{3}\right)\right], \tag{6}$$

$$\alpha_{2,max} = \arctan\left[\frac{2}{\sqrt{3}}\cos\left(\frac{\arccos(-12\sqrt{3}F)}{3}\right)\right]. \tag{7}$$

(2) Pick randomly a value of α_2 between the two limits, $\alpha_2 = \alpha_{2,min} + (\alpha_{2,max} - \alpha_{2,min}) \times z$, where z is a random number between 0 and 1.

(3) The corresponding value of the largest corner half angle α_1 can be found from

$$\alpha_1 = -\frac{1}{2}\alpha_2 + \frac{1}{2}\arcsin\left(\frac{\tan\,\alpha_2 + 4F}{\tan\,\alpha_2 - 4F}\sin\,\alpha_2\right). \tag{8}$$

(4) The smallest corner half angle is then obtained from $\alpha_3 = \pi/2 - (\alpha_1 + \alpha_2)$.

C. Restricting snapoff to throats

In theory it is possible for snapoff to occur in pores. Consider a pore that is connected to two throats. One branch has a wide pore/throat boundary radius and the other has a small pore/throat boundary radius. It is possible that a meniscus passing the wide boundary will cause snapoff at the narrow boundary, as we will describe later in the context of snapoff in throats. This is an unphysical effect. Therefore we limit snapoff to the throats. This can be done by ensuring that the radius at the pore/throat boundary is greater than half the radius at the pore center, Eq. (9),

$$R_{boundary} > \frac{1}{2} R_P. \tag{9}$$

Substituting Eq. (2) in Eq. (9),

$$\left[\left(\frac{R_p + R_t}{2} \right) + \left(\frac{R_p - R_t}{2} \right) \cos\left(\frac{\pi l_p}{l_p + l_t} \right) \right] > \frac{1}{2} R_P. \tag{10}$$

Rearranging,

$$\frac{1}{\pi} \arccos\left(\frac{R_t}{R_t - R_p} \right) > \frac{l_p}{l_p + l_t}. \tag{11}$$

If "=" sign is used in Eq. (11) instead of ">," the final pore length can be given by the following expression:

$$l_{p-final} = (l_p + l_t) \left[\frac{1}{\pi} \arccos\left(\frac{R_t}{R_t - R_p} \right) \right], \tag{12}$$

where $(l_p + l_t)$ represents the spacing between the pore and the throat. If Eq. (11) is not satisfied, the pore length is reduced using Eq. (12) with $(l_p + l_t)$ held constant.

IV. FLUID FLOW THROUGH THE NETWORK

Initially, the system is assumed to be completely filled with a defending, wetting fluid (water) with viscosity μ_2. The invading nonwetting fluid (oil) with viscosity μ_1 is injected into the system from the inlet side with a constant injection rate. The fluids are assumed to be immiscible and incompressible. We assume we have a water-wet system with an oil/water contact angle $\theta = 0$.

A. Determination of fluid configurations

We start by assuming the volume of each phase in each pore or throat is known. Then, with known contact angles, the fluid configuration and the local capillary pressure can be computed.

The total cross-sectional area (A_t) for an element (pore or throat) filled with a single phase is

$$A_t = R^2 \sum_{i=1}^{n} \cot(\alpha_i) = CR^2, \tag{13}$$

where n represents the number of the corners, α is the corner half angle, and C is a constant defined by Eq. (13). Therefore, the volume for a fluid that occupies the whole cross section can be given by the following equation:

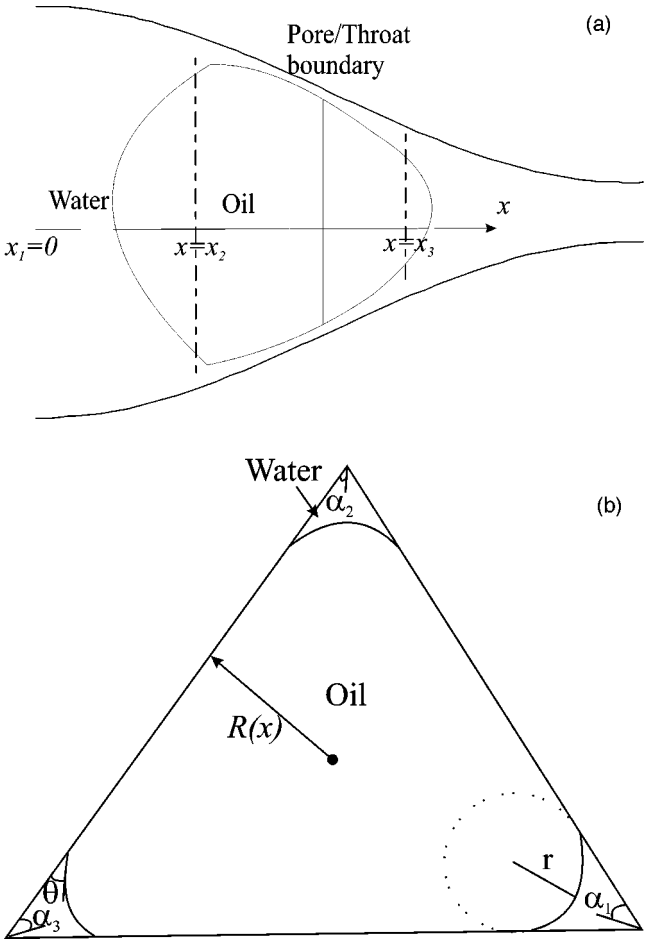

FIG. 2. Illustration of a fluid configuration: oil occupies the pore/throat boundary. (a) Side view: the inscribed radius of the pore element $[R(x)]$ varies sinusoidally with the length. (b) Cross-sectional view at the pore/throat boundary: the pore element has a triangular cross section. Oil is in the center and water is in the corners (wetting layers). θ is the contact angle and r is the radius of curvature of the wetting layers. We assume that r is same in all the three corners and constant in each pore or throat, but varies between pores and throats and over time.

$$V = C \int_{x_1}^{x_2} R^2(x) dx, \tag{14}$$

where $R(x)$ is given by Eq. (2). Here, x_1 and x_2 are the limits of the integration that are determined by the location of the fluid interfaces. For example in Fig. 2(a), the water fills the pore from the center up to the first oil-water interface, so here, $x_1 = 0.0$ and x_2= the location of the interface.

In the case of water in wetting layers and the oil in the center, the wetting layer volume is equivalent to the volume of a cylinder that has cross-sectional area equal to the wetting layer cross-section and length equal to the difference of the location of the fluid interfaces,

$$A_{ci} = r^2\left(\cos\,\theta(\cot\,\alpha_i\cos\,\theta - \sin\,\theta) + \theta + \alpha_i - \frac{\pi}{2}\right), \quad (15)$$

where A_{ci} is the cross sectional area of the ith wetting layer, r is the radius of the curvature of the wetting layer, and θ is the contact angle. The total cross sectional area for all the wetting layers is

$$A_c = \sum_{i=1}^{n} A_{ci}, \quad (16)$$

where n represents the number of the corners.

The oil volume will be the difference between the total volume given by Eq. (14) and the wetting layer volume. For example, in Fig. 2(a), the wetting layer volume between the interface ($x=x_2$) and the pore-throat boundary is obtained by computing the wetting layer cross-sectional area at the location of the interface ($x=x_2$) using Eq. (16) and multiplying it by the difference between the location of the interface and the pore-throat boundary. Equation (14) is used to find the volume between the interface ($x=x_2$) and the pore-throat boundary. The oil volume then will be the difference between these two volumes. For simplicity, in the volume calculations we assume that fluid interfaces, except in the wetting layers, are flat. However, interfacial curvature is accounted for in the computation of capillary pressure.

B. Computing the fluid resistance

Calculating the fluid resistance is potentially a complicated problem, but using an equivalent electrical resistors network helps to simplify the computations. Before giving a detailed description of how the equivalent hydraulic resistance is obtained, it is worthwhile to state the expressions used in finding the resistance of each phase. A phase may occupy: the whole element cross section, the corners with the other (nonwetting) phase in the center, or the center of the element with the other (wetting) phase in the corners. The general form of the fluid hydraulic resistance (W) for the three regions is

$$W = \mu_f \int_{x_1}^{x_2} \frac{dx}{G(x)_{region}}, \quad (17)$$

where the subscript *region* stands for the three regions: whole cross section, center, or wetting layers; x_1 and x_2 are the location of the interfaces; $G(x)$ is the fluid conductance per unit length, and μ_f is the fluid viscosity. The conductance per unit length of a fluid occupying the whole cross section is given by the following approximation based on Poiseuille's law for flow in a circular cylinder [7]:

$$G = \frac{\pi}{128}\left(\sqrt{\frac{A_t}{\pi}} + R\right)^4, \quad (18)$$

where A_t is the cross-sectional area given by Eq. (13) and R is the inscribed radius given by Eq. (2). Since R in Eq. (18) is function of x, the integration in Eq. (17) is evaluated numerically.

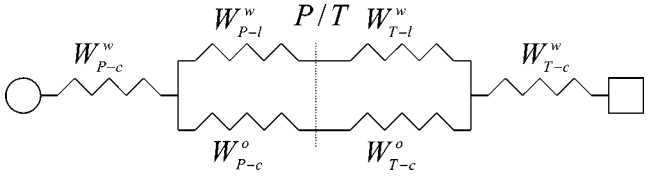

FIG. 3. The equivalent electrical resistors diagram for Fig. 2(a) used to compute hydraulic resistance (W).

In the case where fluid occupies the corners with $\theta+\alpha < \pi/2$, the conductance per unit length is given by the following approximation [33]:

$$G = \sum_{i=1}^{n}\left(\frac{A_{ci}^2(1-\sin\,\alpha_i)^2(\phi_2\cos\,\theta - \phi_1)\phi_3^2}{12(\sin\,\alpha_i)^2(1-\phi_3)^2(\phi_2 + f\phi_1)^2}\right), \quad (19)$$

where $\phi_1 = \pi/2 - \alpha_i$, $\phi_2 = \cot\,\alpha_i\cos\,\theta - \sin\,\theta$, $\phi_3 = (\pi/2 - \alpha_i)\tan\,\alpha_i$, and A_{ci} is the corner area given by Eq. (15). f is used to indicate the boundary condition at the fluid/fluid interface, $f=1$ represents a no-flow boundary, while $f=0$ is a free boundary. In Eq. (19) we assume $f=1$. The curvature of the wetting layer is assumed to be constant in a single element (i.e., G is not function of x), although it varies between pores and throats. Thus we can write the hydraulic wetting layer flow resistance (W_l) as

$$W_l = \frac{\mu_f(x_2 - x_1)}{G}, \quad (20)$$

ignoring the curvature of the pores and throats in the x direction.

When fluid occupies the center of an element with wetting phase in the corners, the conductance per unit length is given by Eq. (18) replacing A_t by A_{cen}, where $A_{cen} = A_t - \Sigma_{i=1}^{n} A_{ci}$, A_{ci} is the corner area, n represents the number of corners.

Using these formulas enables the model to handle any number of fluid interfaces between pore and throat centers. The use of the electrical resistors diagram and equivalent hydraulic resistance simplifies and clarifies this approach. For example, Fig. 2(a) shows a fluid configuration where oil occupies the center at the pore/throat boundary. Its equivalent electrical resistors diagram is given in Fig. 3. Thus the equivalent hydraulic resistance of the fluids between the interfaces ($W_{\text{eq interface}}$) is given by the following equation:

$$\frac{1}{W_{\text{eq interface}}} = \frac{1}{W^w_{P\text{-}l} + W^w_{T\text{-}l}} + \frac{1}{W^o_{P\text{-}c} + W^o_{T\text{-}c}}, \quad (21)$$

where $W^w_{P\text{-}l}$ is the pore wetting layer resistance, $W^w_{T\text{-}l}$ is the throat wetting layer resistance, $W^o_{P\text{-}c}$ is the pore oil resistance, and $W^o_{T\text{-}c}$ is throat oil resistance. Then, the equivalent hydraulic resistance for the fluids between pore and the throat centers (W_{eq}) can be obtained through the following expression:

$$W_{\text{eq}} = W^w_{P\text{-}c} + W_{\text{eq interface}} + W^w_{T\text{-}c}, \quad (22)$$

where $W^w_{P\text{-}c}$ is the pore water resistance and $W^w_{T\text{-}c}$ is the throat water resistance. This is only one example of how the equivalent hydraulic resistance is computed.

The Appendix lists the expressions used for the different fluid configurations considered in the model. We only allow up to two menisci to be present in each throat and one meniscus in each pore branch.

V. SOLVING FOR THE FLUID PRESSURE

Since the equivalent hydraulic resistance is used in the volume conservation equations, the model can be considered as solving a single-phase flow problem in which the phase conductance between the pore and throat centers is found from the equivalent hydraulic resistance calculated in the previous step. Therefore, the total flow rate between the pore center and throat center will be

$$Q_{\text{total}} = \frac{P_p - P_t + P_c}{W_{\text{eq}}}, \tag{23}$$

where P_p and P_t are the pore center pressure and throat center pressure, respectively, P_c is the sum of the capillary pressures of the menisci between the pore and throat centers. For instance, in Fig. 2(a), $P_c = P_{c1} + P_{c2}$, where, P_{c1} is the capillary pressure at the first interface ($x = x_2$) and P_{c2} is the capillary pressure at the second interface ($x = x_3$). The absolute value of the capillary pressure at any meniscus is given by the following expression:

$$P_c = \frac{2\sigma \cos(\theta + \gamma)}{R(x)}, \tag{24}$$

where γ is the inclination angle; $\tan \gamma = dR(x)/dx$. The sign of the capillary pressure at any meniscus depends on the location of the nonwetting fluid (oil). If it is on the right of the meniscus, the sign is positive, otherwise it will be negative.

For a system of m throats and n pores, we have $m+n$ unknowns. These unknowns are determined by applying volume conservation for both the pores and throats. The conservation equation for pore j with n connecting throats, labeled, i is

$$\sum_{i=1}^{n} Q_{\text{total}}^{ij} = \sum_{i=1}^{n} \frac{P_p^j - P_t^i + P_{cij}}{W_{\text{eq}}^{ij}} = 0. \tag{25}$$

For a throat i, where R and L label the left and right pores,

$$\frac{P_p^R - P_t^i + P_c^{Ri}}{W_{\text{eq}}^{Ri}} + \frac{P_p^L - P_t^i + P_c^{Li}}{W_{\text{eq}}^{Li}} = 0. \tag{26}$$

We use Eq. (26) to find the throat pressures that are then put in Eq. (25) to obtain a series of linear equations for pore pressures only. Once the pore pressures have been found, Eq. (26) can be used to compute the throat pressures. Equation (25) is solved using a standard iterative matrix solver.

The pressures are used to compute the phase flow rates across the pore/throat boundaries. For example, from the equivalent resistors diagram of Fig. 2(a), the water flow rate across the pore/throat boundary is the wetting layer flow rate and it is given through the following equation:

$$Q_{\text{water}} = \frac{(P_p - P_t + P_c)}{W_{\text{eq}}(W_{P\text{-}l}^w + W_{T\text{-}l}^w)}[W_{\text{eq}} - (W_{P\text{-}c}^w + W_{T\text{-}c}^w)]. \tag{27}$$

The oil flow rate is

$$Q_{\text{oil}} = Q_{\text{total}} - Q_{\text{water}}. \tag{28}$$

Solving for constant injection rate

While we set up the pressure equation for constant inlet and outlet pressures we want to simulate flow with a constant injection rate. Aker *et al.* [25] have shown how to achieve a constant injection rate in a dynamic network model. However, their method involves solving for the pressure field twice at each time step. Here we use an approximate technique that only requires a single pressure solution. Over time the pressure drop across the network changes. We assume that between time steps the change in pressure drop necessary to maintain a constant injection rate is small. Hence we simply adjust the pressure drop at each time step to maintain a constant value of Q as follows.

(a) For the nth time step, the pore and throat pressures are computed as described above, with a pressure drop ΔP^n.

(b) The total injection rate (Q^n) is then obtained by summing all the flow rates between the inlet throats and their connected pores.

(c) For the next pressure solve, for the $(n+1)$th time step we use a pressure drop

$$\Delta P^{n+1} = \Delta P^n \times \left[1 + \beta\left(\frac{Q_{\text{desired}} - Q^n}{Q_{\text{desired}}}\right)\right], \tag{29}$$

where Q_{desired} is the desired, target injection rate and β is a constant parameter, which we set to 0.5. This method maintained Q^n to within 0.5% of Q_{desired} for the cases we studied.

VI. SELECTION OF THE TIME STEP

We choose a time step (Δt) according to the following formula:

$$\Delta t = \min\left\{5 \times 10^{-5}\ \text{s}, \min\left\{\frac{V_i}{2Q_i}\middle| i = 1, \ldots, n\right\}\right\}, \tag{30}$$

where n is the number of the elements in the pore network, V_i is the ith element volume (i.e., the maximum amount of fluid that can be held in the ith element), and Q_i is the total flow rate into the ith element. Equation (30) ensures that an element cannot be completely filled in a single time step. The time step value of 5×10^{-5} s ensures that in most cases only a small fraction of a volume of a pore or throat is filled with invading fluid in a time step.

VII. UPDATING FLUID VOLUMES

Once the fluid volumes are determined, the configuration of the phases in the elements is adjusted. There are two steps in this process. First, the pressure computation only determines the total flow of oil and water between pore and throat

centers—we need to use the fluid configuration to determine the flow rates of each phase from pore to throat. Having done this the water volume in each element is updated. From the new fluid volume the configuration of each phase in each element is determined and a new total fluid resistance can be found, the pressure recomputed, and the simulation continues. For example, consider the fluid configuration shown in Fig. 2(a). From the total flow rate across the pore/throat boundary, Eq. (23), and assuming that the flow direction is towards the throat, the water flow rate in the throat ($Q^{\text{in}}_{\text{water}}$) is given by Eq. (27) and is small, since this is only flow in layers. Similarly we can compute the flow rate of water out of the throat at the pore/throat boundary to the right of the throat center ($Q^{\text{out}}_{\text{water}}$). The new water volume in the throat for time level n is given by the following expression:

$$V^{n}_{\text{water}} = V^{n-1}_{\text{water}} + (Q^{\text{in}}_{\text{water}} - Q^{\text{out}}_{\text{water}}) \times \Delta t. \tag{31}$$

Then Eq. (14) is reused to find the new location of the interface, with $V = V^{n}_{\text{water}}$ and $x_2 = (l_p + l_t)/2$ (i.e., the throat center). It is clear that the interface location cannot be obtained from a direct substitution, and so an iterative method must be used to obtain an interface location consistent with the imposed change in volume.

To recap: the capillary pressure in each pore or throat is constant, but varies between pores and throats. In any one element the capillary pressure determined from the curvature of the wetting layers (σ/r where r is the radius of curvature of the wetting layers) is the same as the capillary pressure determined at the interface between oil and water in the center of the element, Eq. (24). This enables a unique determination of fluid configuration from the known volume of wetting phase.

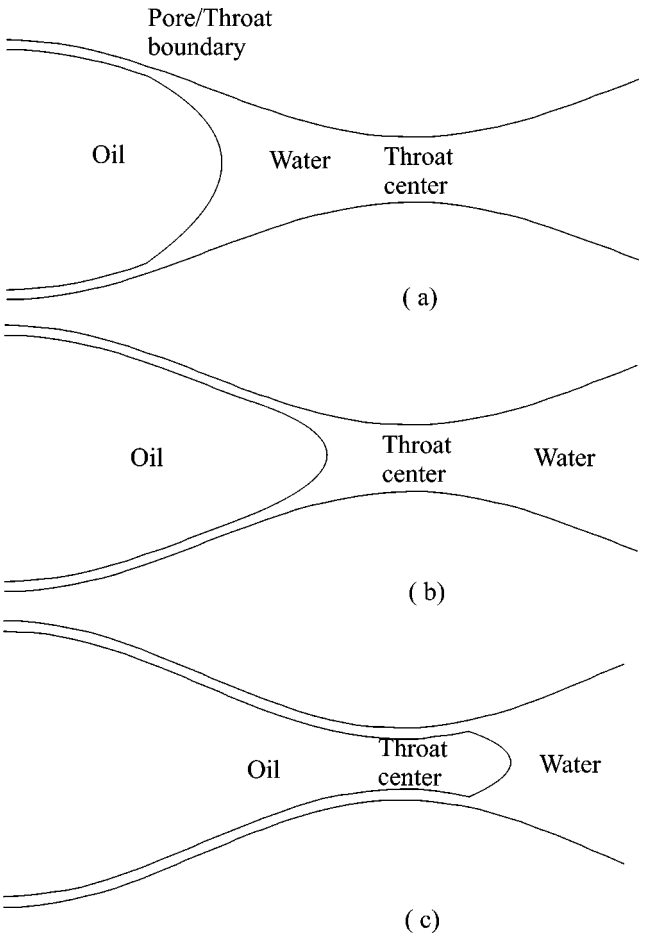

FIG. 4. Invasion of a single pore branch or throat side. (a) Oil is filling the pore branch. (b) Oil is entering the throat side. (c) Oil is passing the throat center.

VIII. MICROFLOW MECHANISMS OF PRIMARY DRAINAGE

The fluid displacement mechanisms can be divided into two main types: pistonlike and snapoff. The purpose of this section is to explain how the model can be used to simulate the pore-level processes that have been seen in micromodel experiments [14].

A. Pistonlike displacement

This is the process by which the displacing fluid pressure is high enough to allow the displacing fluid to enter the bulk of the pore element by pushing the displaced fluid in front of it. There are three types of pistonlike invasion: invasion of a single pore branch or throat side, invasion of a pore center, and menisci fusion.

1. Invasion of a single pore branch or throat side

This type of invasion occurs if the pressure of the element that contains the displacing fluid is higher than the pressure of the connected element that contains the displaced fluid plus the local capillary pressure. For example, Fig. 4(a) shows a pore branch whose center is filled with oil and a throat that is fully water saturated. If the pore pressure is higher than the summation of the throat pressure and local capillary pressure, the oil advances towards the throat center [Fig. 4(b)]. The amount of oil that enters the throat is controlled by the pressure difference between the pore and the throat and the pore-throat geometries. The oil continues moving until it passes the throat center and starts filling the other side of the throat [Fig. 4(c)].

This mechanism is modeled by changing the fluid configurations according to the location of the oil/water interface. Figure 5 shows a simplified flow chart of how this is done. From Fig. 4, it is clear that this mechanism involves two fluid configurations: where the meniscus is between the left pore and the throat center, and where the meniscus is between the throat and the right pore center. The equations for the fluid equivalent resistance, phase fluxes and field pressures for both configurations are provided in the Appendix. If the volume of oil that enters the system (displaced volume) is positive, the oil will enter the throat, otherwise, the fluid configuration remains unchanged. If oil enters the throat, the volume of the oil in the throat and the new location of the oil/water interface are determined according to the procedure explained in the preceding section. If the new in-

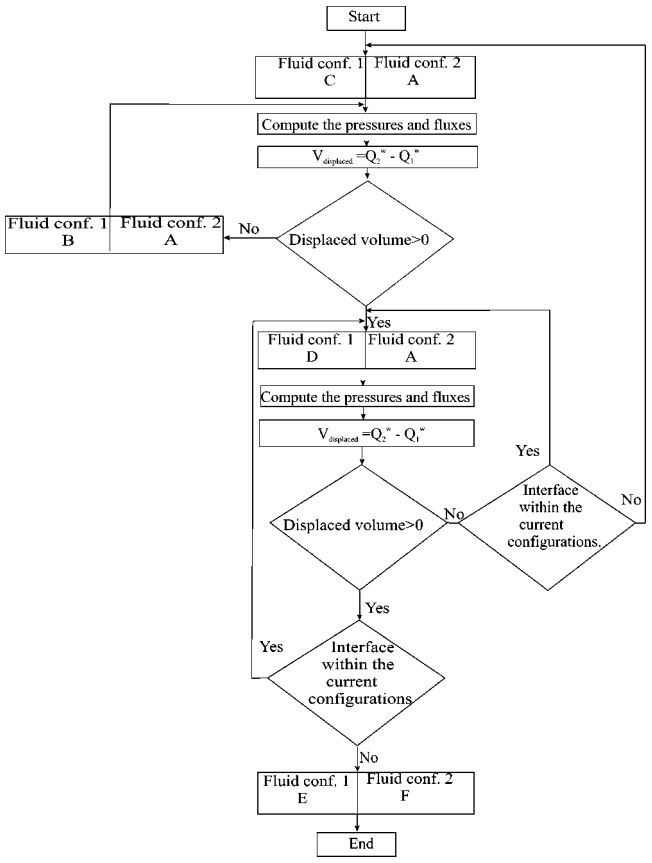

FIG. 5. Flow chart of oil invasion of a single pore branch shown in Fig. 4. The fluid configurations mentioned are explained in the Appendix.

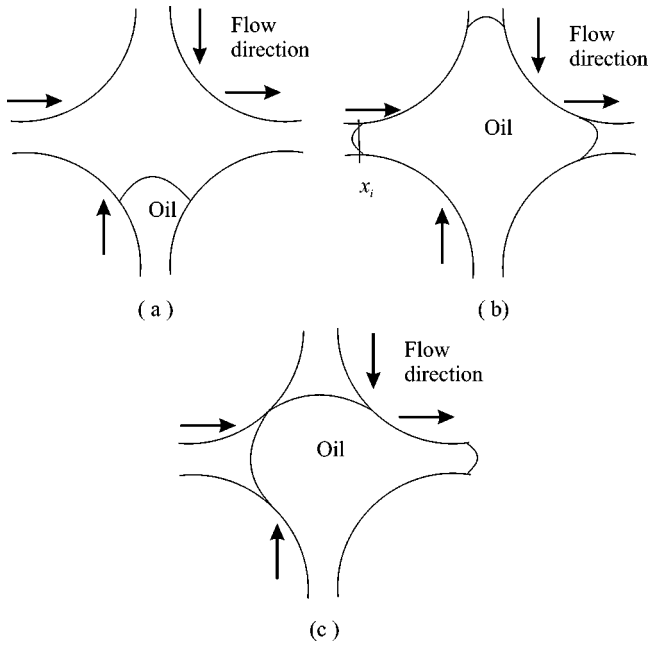

FIG. 6. Oil invasion of a pore center. (a) Oil approaching the pore center. (b) When the volume of oil flowing into the pore exceeds the volume of the lower branch, oil is distributed in all branches, regardless of flow direction. The capillary pressure in all the branches is same. (c) In the subsequent time steps the oil interfaces are updated according to the local flow direction.

terface cannot be located to the left of the throat center, the fluid configuration will be changed to one in which the location of the new interface has moved beyond the center of the throat, as shown in Fig. 4.

2. Invasion of a pore center

When an interface reaches the pore center, it is moved into the neighboring flow channels. Consider the diagram shown in Fig. 6(a). If the oil volume entering from the lower branch is more than the water that is displaced from the branch, the remaining oil will be distributed among all the connected branches regardless of whether these branches are connected to a throat with higher or lower pressure than the pore pressure (i.e., regardless of the flow direction), Fig. 6(b). The remaining oil is distributed so that there is the same capillary pressure at the interfaces in all the connected branches. Then in subsequent time steps, the oil will move in the flow direction, Fig. 6(c). In summary:

(1) Check if the remaining oil is more than the summation of the connected branches volume. If this is so, the whole pore is filled with oil, otherwise we move to the next step.

(2) Sort the branches according to their size. The branch with the smallest size is at the top of the list and the one with the largest size is at the bottom of the list.

(3) We make an initial guess of the location of the interface in the branch of the smallest size that is used to find the capillary pressure in the branch. Then, by maintaining the same capillary pressure in all other branches, the location of the interfaces in these branches will be found using an iterative method.

(4) The total volume can be given by the following expression:

$$V = \sum_{i=1}^{m} [V_i(x)]_{x_2=x_i}^{x_1=0}, \tag{32}$$

where $V_i(x)$ is given by Eq. (14), x_i is the location of the interface in the ith branch obtained from step (2), and m is the number of branches.

(5) Check if the volume obtained in step (4) is equal to the volume of the remaining oil. If it is, these are the right locations for the interfaces, otherwise steps (3) and (4) are repeated again until the correct locations are reached.

3. Menisci fusion

Menisci fusion is an oil invasion mechanism in which a throat that connects two fully oil-filled pore branches holds two menisci back to back that come together. The fusion of two menisci in a throat is straightforward to model and occurs when the interface locations coincide, at which point all the water volume is accommodated in layers. However, more complex situations may arrive if both oil and water are flowing in the same direction through a throat, as shown in Fig. 7.

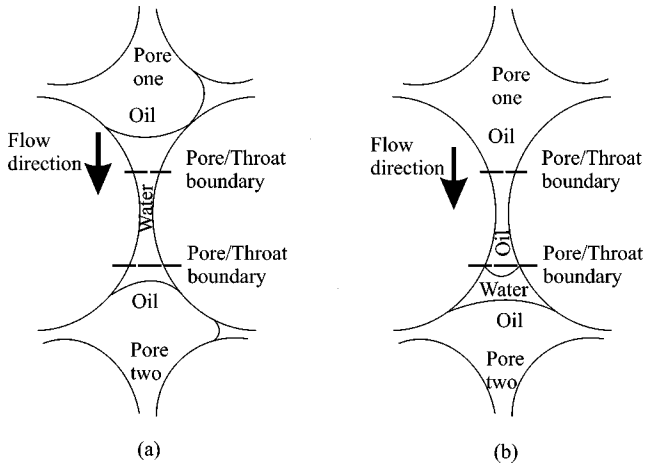

FIG. 7. Oil invasion. (a) Oil begins to invade a throat. (b) Invasion may continue until the meniscus reaches the pore/throat boundary. We do not allow two menisci in a single pore branch. Hence the meniscus remains frozen in place until the water volume in pore two is insufficient to support occupancy of the element center. Then the menisci fuse, and water only occupies layers.

This is the typical situation at high capillary numbers. Oil displaces water through a throat in a pistonlike fashion until the oil/water meniscus reaches the pore/throat boundary, Fig. 7(b). In reality further displacement would lead to there being two menisci in the pore branch. However, this is not allowed in our model. Instead we freeze the meniscus at the pore/throat boundary. We assume that the flux from the element center into pore two is from oil. However, we keep the interface location fixed until the water volume is too small to be accommodated in the pore center and the two menisci fuse leaving water only in layers.

B. Snapoff

Snapoff is a mechanism that is controlled by wetting layer flow. Water accumulates in layers until oil no longer contacts the solid and water spontaneously fills the center of the throat, separating the oil into two droplets. The accumulation of water in the wetting layers is function of the contact angle and the pore/throat aspect ratio.

In our model, there are two types of snapoff. Snapoff that occurs to the oil that invades a fully water-saturated throat will be called snapoff in drainage. The second snapoff occurs in a throat that is already filled with oil. Here, the water starts accumulating in the wetting layers as a result of a drop in the capillary pressure. Many authors have described this process (see for instance, Blunt *et al.* [4] and Mogensen and Stenby [30]). This type of snapoff will be called snapoff in imbibition, since it is common in imbibition. However, there is nothing preventing it from happening in drainage, as mentioned by Toledo *et al.* [34].

1. Snapoff in drainage

When the nonwetting phase invades a fully water-saturated throat, the wetting phase will remain in the corners. As the nonwetting fluid passes the narrowest section of the throat, the radius of the curvature of the wetting layers will be at its smallest value. Then, with increasing oil volume in the throat, the meniscus is pushed into wider regions, the capillary pressure decreases and the wetting phase in the layers starts to accumulate (see Fig. 8). This process may continue until the wetting fluid cannot be held in the wetting layers any more. At this point, it will snapoff at the narrowest pore of the throat separating the oil into two droplets.

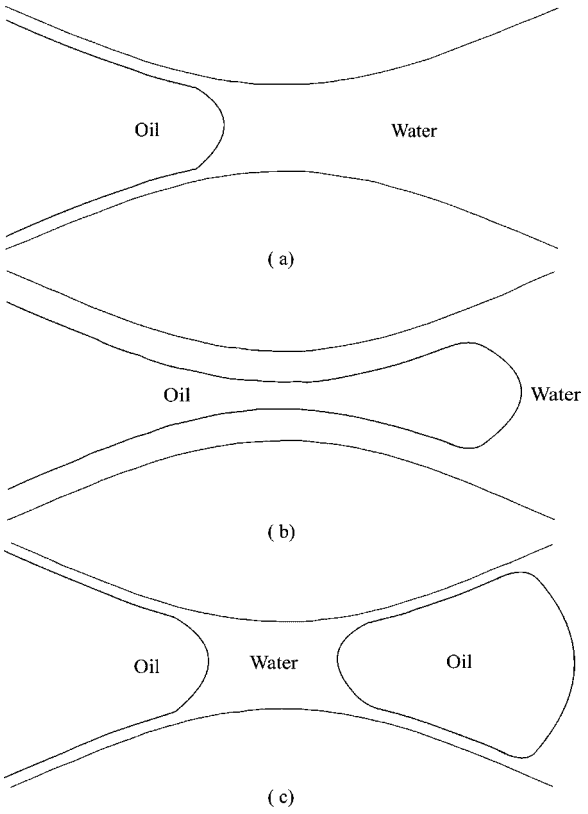

FIG. 8. Snapoff in drainage. (a) Oil is approaching the narrowest region of the throat. (b) Water in wetting layers accumulates when the capillary pressure drops as oil advances into wider regions of the throat space. (c) Water snaps off at the center of the throat separating the oil into two droplets.

If the volume of water flowing into the throat is more than the water flowing out in Fig. 8(c), the volume of water in the center of the throat will increase and after snapoff water will fill the whole throat cross section at its narrowest point. This means that oil will enter the throat but it cannot penetrate it. If the water flow into the throat is less than that flowing out, the volume of water in the center will shrink until the two oil menisci meet, reconnecting the oil, and the oil then continues flowing to the next pore.

2. Snapoff in imbibition

If the water flowing into an oil-filled throat through wetting layers is more than that flowing out, water accumulates in the wetting layers [see Fig. 9(a)]. This accumulation process might eventually lead to snapoff [Fig. 9(b)].

Our strategy for modeling this type of snapoff is illustrated in Fig. 10. Snapoff occurs when the volume of water at the narrowest part of the throat is too large to be accommo-

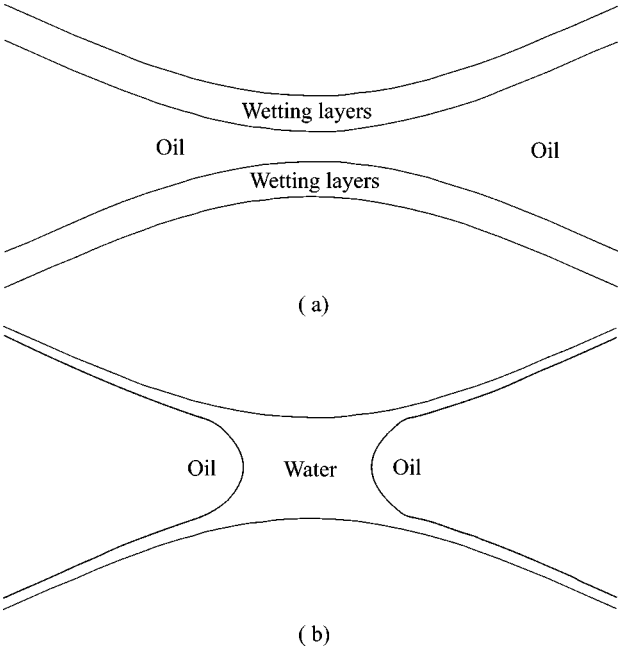

FIG. 9. Modeling snapoff in imbibition. (a) Water accumulates in the wetting layers. (b) Water snaps off at the center of the throat.

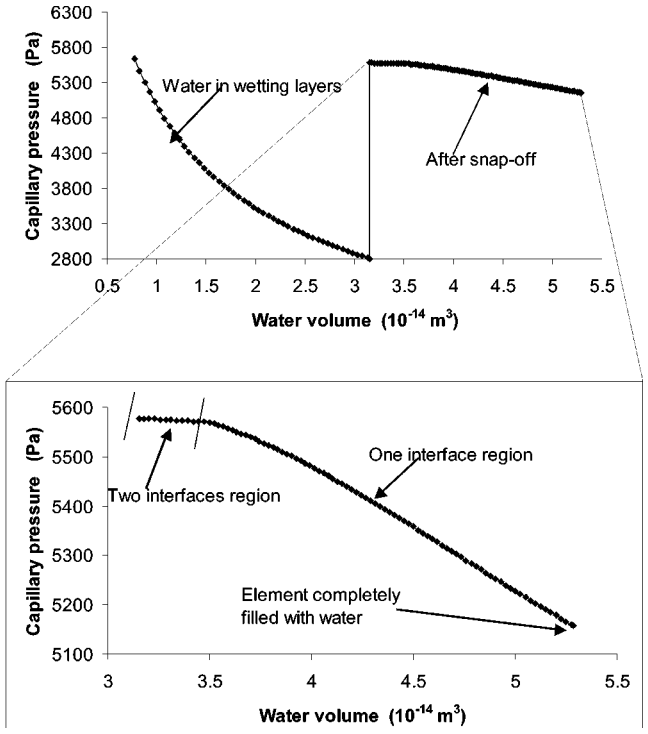

FIG. 10. Modeling snapoff in imbibition. Capillary pressure is shown as a function of water volume for an example throat. When the water volume in the throat is sufficiently large, the water can only be accommodated by having the center of the throat completely filled with water—this represents snapoff.

dated in layers. At this point water spontaneously and instantly fills the center of the throat and the oil is separated into two. Notice that when this happens the local capillary pressure increases.

IX. SIMULATIONS

The flow is characterized by two dimensionless numbers: the capillary number Ca, Eq. (1), and the viscosity ratio M, which is defined as the ratio between the defending fluid viscosity μ_2 and the invading fluid viscosity μ_1,

$$M = \frac{\mu_2}{\mu_1}. \tag{33}$$

In this work, we divide our results under three categories: the influence of capillary number on the dynamic fluid movement, the relation between the capillary number (flow rate), and the snapoff phenomenon and the influence of viscosity ratio.

A. Influence of capillary number on the dynamic fluid movement

In this subsection, we change the capillary number by varying the injection flow rate. The general understanding of oil invasion is that at high capillary numbers the oil fills all the pore elements regardless of size and moves towards the outlet face in a pistonlike fashion [14]. However, at low capillary number, the oil flows through a pathway of larger pores and throats with the lowest capillary entry pressure. This leads to a ramified, invasion percolationlike displacement that can be simulated readily with quasistatic models [14,15]. In this section we will test whether or not our model reduces to the quasistatic limit as the flow rate is decreased.

Figure 11 shows the fluid distribution for simulations at different capillary number (oil is shown in gray and water in black). In all the simulations, we used a two-dimensional (2D) network of 9×9 pores, a unit viscosity ratio (fluid viscosity of 1 Pa s), and 0.05 Nm^{-1} interfacial tension. The selection of this network size is based on optimization of the computation time that is required to complete the runs. The run for the lowest capillary number ($\mathrm{Ca}=3.1\times10^{-5}$) took around 55 h on a standard PC. The runs were stopped at first oil breakthrough. The Darcy oil velocity is obtained by dividing the oil injection rate by the inlet cross sectional area. The oil injection rate is the sum of the oil flow rates between the inlet throats and the connecting pore branches. The inlet cross sectional area (0.52 mm^2) is the product of the length of the inlet (2600 μm) and the mean thickness of the lattice which is taken to be the average diameter of the pores (200 μm). Each simulation was performed at a constant injection rate. In the pictures shown in Fig. 11, each pore is connected to four throats and a small black line is used to distinguish between the pore branch and the throat. In addition, when snapoff occurs there are throats having two interfaces (water occupies the throat center). Figure 11(a) shows the results of a quasistatic model that ignores rate-dependent effects for the same network (9×9 pores) [28] to compare it with the dynamic one at the lowest capillary number Ca $=3.1\times10^{-5}$ [Fig. 11(b)].

As the capillary number is increased, the oil flows through more of the inlet pores and sweeps more of the network, although there is an increasing frequency of snapoff. At the

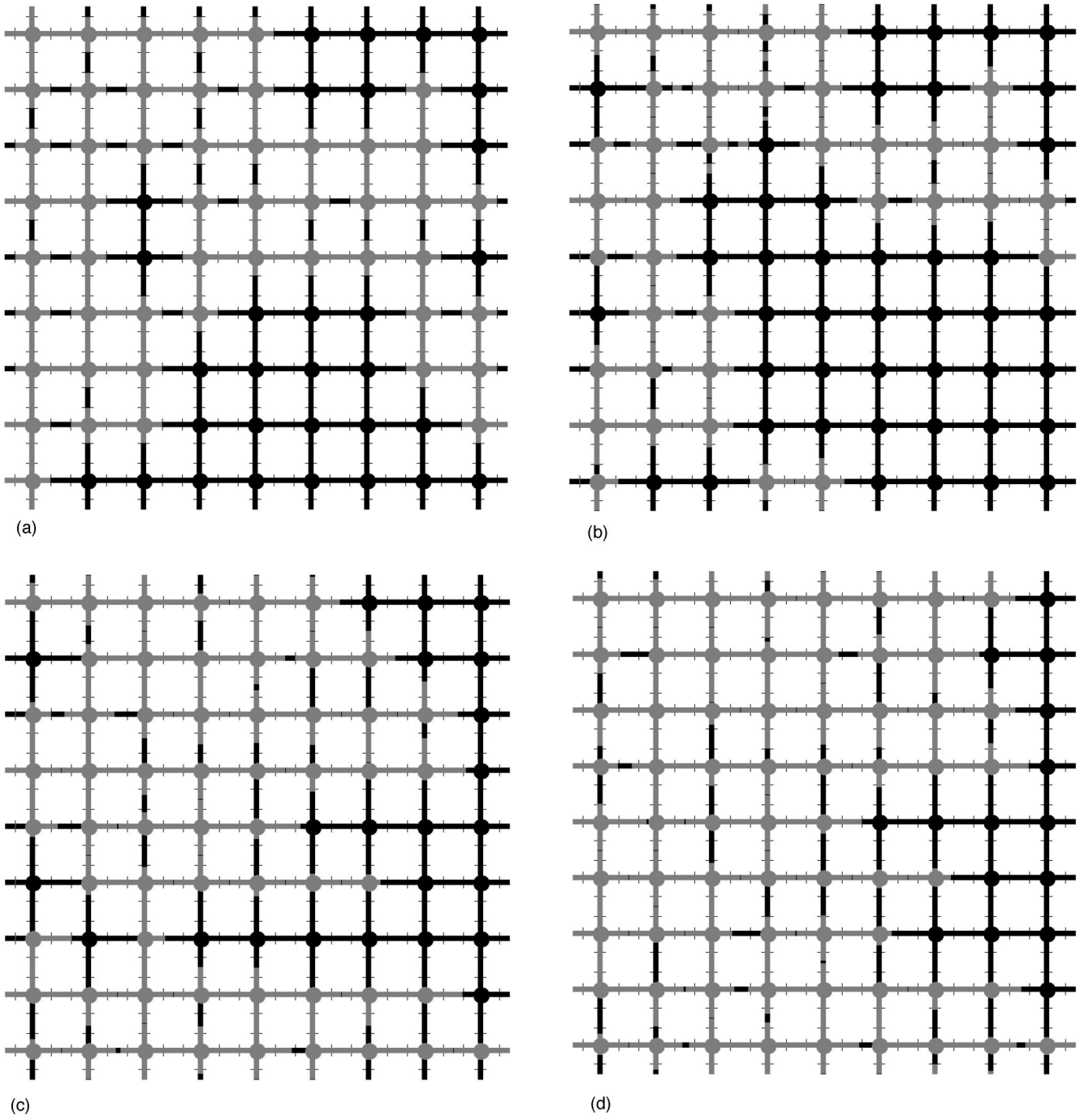

FIG. 11. Fluid distributions for simulations of primary drainage at different capillary number (Ca). In this and subsequent figures, the water in the centers of pores and throats is shown in black and oil is shown in gray. The fine black lines separate pores and throats. The distributions at oil breakthrough are shown. (a) A quasistatic model, representing the limit of $\mathrm{Ca}\rightarrow 0$. (b) A run for $\mathrm{Ca}=3.1\times 10^{-5}$. (c) $\mathrm{Ca}=3.8\times 10^{-4}$. (d) $\mathrm{Ca}=0.33$.

lowest capillary numbers, the displacement is dendritic and the sequence of pores and throats are filled is largely controlled by their entry capillary pressure (determined by the minimum inscribed radius of the throat). The displacement patterns for $\mathrm{Ca}=3.1\times 10^{-5}$ and $\mathrm{Ca}\rightarrow 0$ are similar, although not identical, since the perturbative effect of viscous forces does affect the exact pathway of filled pores and throats, especially away from the inlet. As the flow rate increases, viscous forces become more significant and small pores near the inlet may be filled in preference to larger pores or throats near the outlet, because of the significant pressure drop across the network. Furthermore, dynamic events, such as snapoff, become more common, and the oil is not necessarily connected to the inlet, although it is still flowing. At the

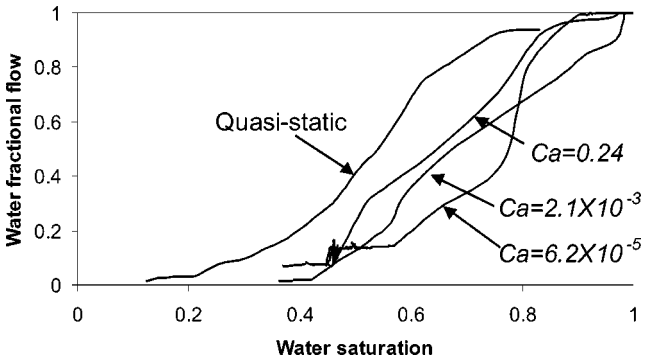

FIG. 12. Water fractional flow as a function of water saturation for different capillary numbers.

highest capillary number studied, 0.33, oil moves largely indiscriminately through pores and throats of any size as a train of generally disconnected ganglia.

1. Fractional flow curves

The fractional flow of phase i in a multiphase system can be given through the following expression:

$$f_i = \frac{Q_i}{Q_{\text{total}}}. \tag{34}$$

In our model, we used a small 2D network (17×17 pores) to study the influence of the capillary number on the fractional flow curves. The computer time needed to model the dynamics of wetting layer flow precluded the use of a larger network. The average saturation was computed in a slice of four-pore length distance at the middle of the network. The phase and total flow rates were obtained at the center of the slice by using the equations provided in the section on solving the fluid pressure.

Figure 12 shows the water fractional flow as a function of water saturation for different capillary numbers. If viscous forces were completely dominant, with oil and water flowing together, then we expect $f_w = S_w$ [2,13,15]. Even at the higher capillary numbers, the effect of wetting layer flow and the wide pore size distribution prevent the fractional flow becoming linear. However, as Ca increases, f_w does tend towards a straight line.

At low capillary number, when capillary forces dominate, the oil and water occupy different pathways (see Fig. 11) with little movement at most oil/water interfaces. As the capillary number increases, more menisci become mobile. This explains why the fractional flow decreases with decreasing capillary number and has an S shape, characteristic of low-rate experimental measurements at the lowest values [2]. While the fractional flow curves for the quasistatic model, $\text{Ca} \to 0$, and $\text{Ca} = 6.2 \times 10^{-5}$ have a similar shape, the quasistatic curve appears to be shifted to lower water saturation which is a result of the difference of the water saturation in wetting layers. In the quasistatic model the capillary pressure is the maximum local entry pressure reached during a displacement—this means that wetting layers tend to carry relatively little water. In contrast, the dynamic model allows locally lower capillary pressures with large amounts of water

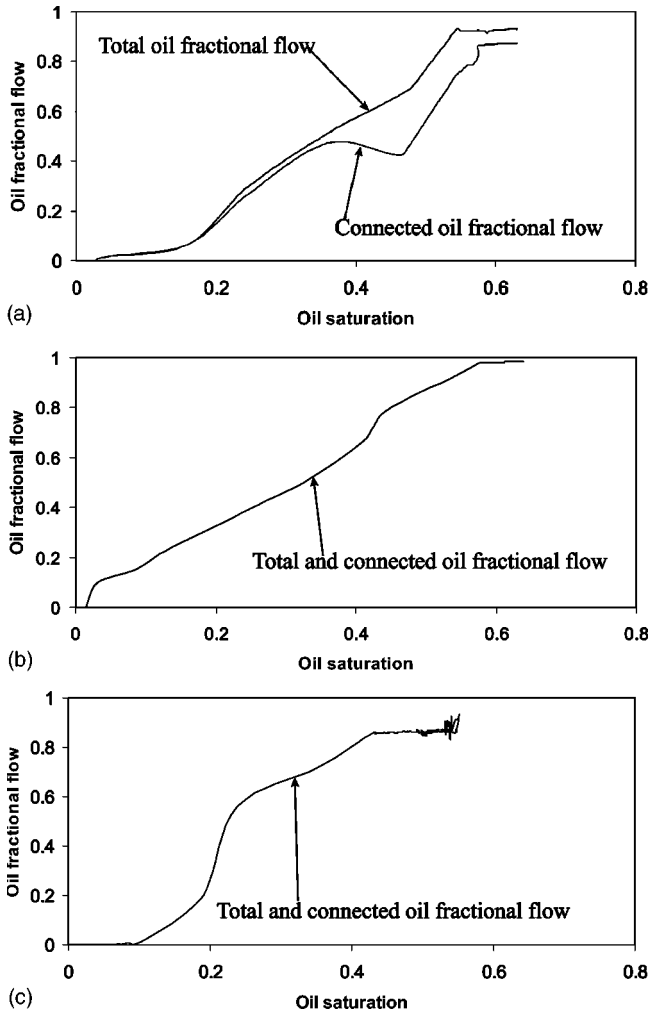

FIG. 13. The oil fractional flow and oil fractional flow from oil connected to the inlet as a function of oil saturation for several capillary numbers. (a) $\text{Ca} = 0.24$, (b) $\text{Ca} = 2.1 \times 10^{-3}$, (c) $\text{Ca} = 6.2 \times 10^{-5}$.

retained in layers. However, these layers carry relatively little flow. For instance, Fig. 10 shows that up to half the total volume of a typical throat may be filled with water in layers. In other words, for a specific value of fractional flow in Fig. 12, the water saturation in wetting layers for the quasistatic model is lower by around 0.2 than that for the dynamic model ($\text{Ca} = 6.2 \times 10^{-5}$). While our model may tend to overestimate the effects of wetting layer flow, it does indicate that the amount of water contained in layers is very sensitive to dynamic effects and may not be accurately predicted by static models.

2. Connected and disconnected flow

Snapoff causes oil to become disconnected in primary drainage. The resultant oil ganglia can flow through the network. The contribution of ganglion transport to the overall flow of oil is represented by the difference between the total oil and connected oil fractional flow curves in Fig. 13. The connected oil fractional flow only considers the flow of oil that is connected to the inlet. It is clear that disconnected

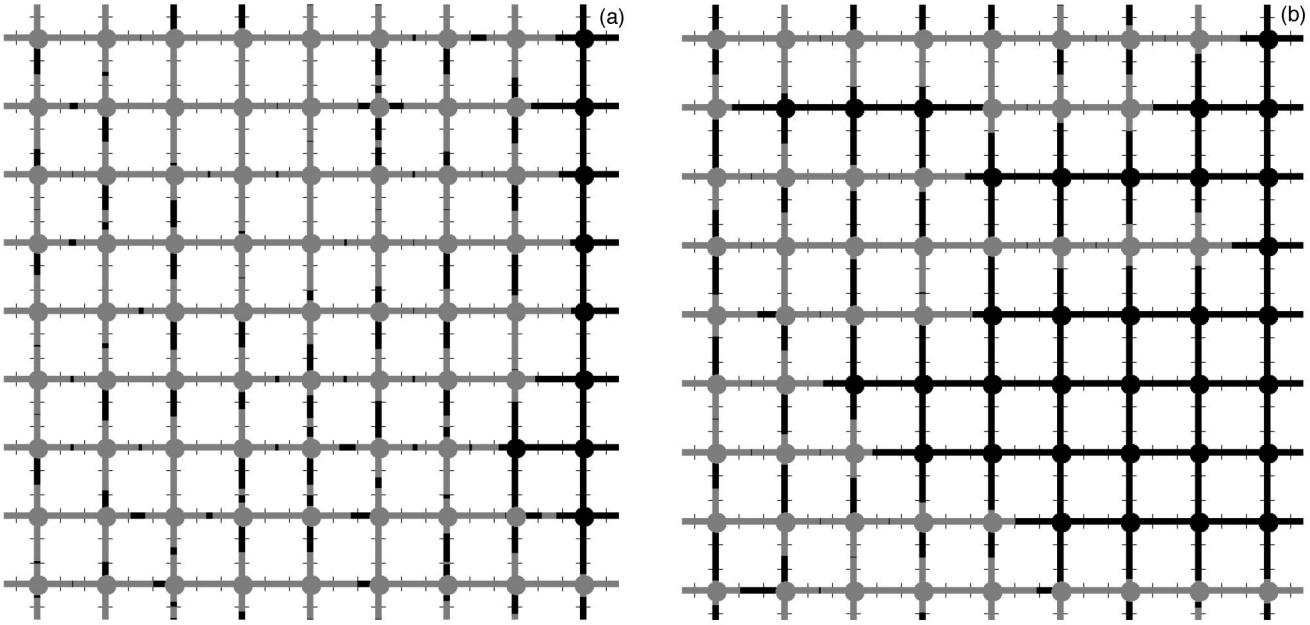

FIG. 14. Influence of viscosity ratio on fluid movement for $Ca=8.3\times10^{-2}$: (a) $M=0.1$; (b) $M=10$.

flow is only appreciable for the largest flow rates, and it is insignificant for most typical reservoir displacements. This contradicts the finding of Payatakes and co-workers who studied two-phase flow behavior in imbibition and found significant ganglion transport for low capillary numbers [18,20]. Our model, however, has a wider pore size distribution and accounts explicitly for wetting layer flow and simulates accurately the dynamics of layer swelling and snapoff. Furthermore, we only consider drainage.

B. Influence of viscosity ratio on fluid movement

In this subsection, we study the effect of viscosity ratio on displacement patterns and the degree of snapoff. For illustrative purposes we ran simulations with a capillary number of 8.3×10^{-2} on the same 9×9 network as before. We also ran a series of simulations on a statistically similar 30×30 network with a capillary number of 1.1×10^{-2}.

At high flow rates and viscosity ratios less than 1 (oil more viscous than water), it would be expected that the displacement of oil by water would be stable, with a relatively flat front progressing through the system. Figure 14(a) illustrates a displacement for $M=0.1$ that confirms this. However, there is a significant amount of snapoff and a significant proportion of the oil moves as disconnected ganglia. The reason for large amounts of snapoff can be explained by studying the fluid resistance of a pore element that contains oil in the center and water in wetting layers. As explained in the section on computing the fluid resistance, the phase resistance is a combination of the geometry (i.e., whether the phase occupies the center, layer, or whole pore) and viscosity. Therefore with an oil viscosity ten times higher than the water viscosity, in the large pores, the oil resistance will be of the same order of magnitude as the wetting layers. This means that the oil flow is relatively slow compared to the accumulation of water in wetting layers. Thus water has sufficient time to accumulate and snapoff at the center, leading to the generation of the oil ganglia seen in Fig. 14(a).

For a viscosity ratio greater than one ($M=10$), the oil fingers through the water [Fig. 14(b)], since the displacement is now unstable. In addition, the wetting layer flow is less significant compared to oil flow in the pore centers, since the water is relatively more viscous, and as a consequence there is less snapoff.

Figure 15 shows the total oil fractional flow and the oil fractional flow considering only the movement of oil that is connected to the inlet for a 2D network of size of 30×30, for (a) $M=0.1$ and (b) $M=10$. For $M=0.1$, snapoff is common and an appreciable amount of oil transport is from disconnected oil [Fig. 15(a)]. In the case of $M=10$, the oil fingers into the water through the larger pores and throats, which means a high oil fractional flow is reached at low oil saturation. In addition, there is not much difference between the total oil fractional flow curve and the continuous one which indicates less occurrence of snapoff.

X. CONCLUSIONS

A dynamic pore network model for simulating two-phase flow in porous media has been developed that accounts for flow in wetting layers. This model predicts the events that are observed in micromodel experiments, such as swelling of the wetting layers, snapoff and meniscus oscillations [14]. The model is based on an idealization of the pore space as a network of pores and throats with triangular cross sections whose inscribed radii vary sinusoidally. The transient pressures were computed at the center of each pore and throat and the locations of the interfaces were updated by using a modified Pouiseuille equation in which an equivalent hydraulic resistance between the pore and throat centers was used.

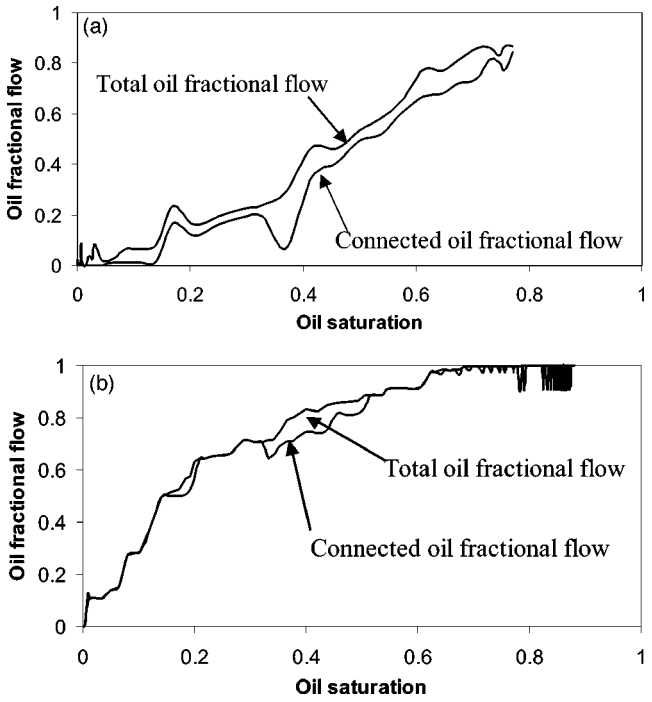

FIG. 15. Influence of viscosity ratio on fluid movement for Ca $=1.1\times10^{-2}$. (a) The total oil fractional flow and connected oil fractional flow curves for $M=0.1$. (b) The total oil fractional flow and connected oil fractional flow curves for $M=10$.

Numerical results were presented for two-dimensional simulations of primary drainage. From these results we conclude the following.

(a) At low capillary number ($Ca\leqslant10^{-5}$), oil tends to flow through the larger pores that have the smallest capillary entry pressures and the displacement pattern is similar to that predicted using a quasistatic model. With increasing capillary number, the oil can enter pores and throats of all sizes and the displacement is less ramified.

(b) More oil ganglia are formed by snapoff as the capillary number increases. However, the contribution of ganglion transport to the overall flow of oil is insignificant except at very large capillary numbers, $Ca>0.1$. This implies that for most reservoir displacements the traditional Darcy-like conceptualization of multiphase flow, that ignores ganglion transport, is reasonably accurate. However, the fractional flow is a function of flow rate for capillary numbers greater than 10^{-5}. The dynamic model, even at the lowest capillary number studied (6.2×10^{-5}), predicted a much greater saturation of water in layers than an equivalent quasistatic model ($Ca\rightarrow0$). This tended to shift the computed water fractional flow curves to the right.

(c) With a viscosity ratio less than one (oil more viscous than water) and high flow rates, a flat frontal displacement is observed but with a large number of oil ganglia. These ganglia are formed by snapoff, which is favored due to the comparatively low flow resistance in wetting layers.

(d) For a viscosity ratio greater than one the oil fingers through the water, there is less snapoff and the oil is well connected.

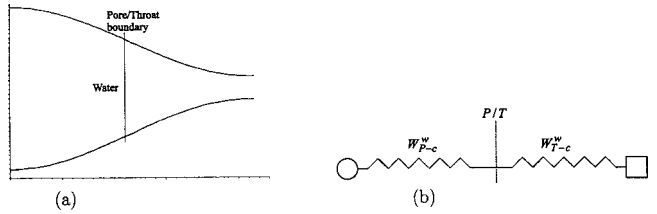

FIG. 16. (a) Fluid configuration A: all water. (b) The equivalent electrical resistors diagram.

ACKNOWLEDGMENTS

We would like to thank PDO Oman and the members of the Imperial College Consortium on Pore-Scale Modelling for financial support.

APPENDIX: FLUID CONFIGURATIONS

There are six main fluid configurations in this model. They are as follows:

(1) *Fluid configuration A.*

In this fluid configuration, the whole unit cell (i.e., pore branch + throat side) is completely filled with water [Fig. 16(a)]. Its equivalent electrical diagram is shown in Fig. 16(b), where the circle and the rectangle stand for the pore center and the throat center, respectively. $W^w_{P\text{-}c}$ is the pore water resistance, P/T is the pore/throat boundary, and $W^w_{T\text{-}c}$ is the throat water resistance.

The total equivalent hydraulic resistance, water equivalent hydraulic resistance, and oil equivalent hydraulic resistance of this fluid configuration is given through Eq. (A1), while Eq. (A2) represents the total flow rate, water flow rate, and oil flow rate:

$$W_{\text{eq}} = W^w_{P\text{-}c} + W^w_{T\text{-}c},\ W^w_{\text{eq}} = W_{\text{eq}},\ W^o_{\text{eq}} = 0.0, \tag{A1}$$

$$Q_{\text{total}} = \frac{P_P - P_T}{W_{\text{eq}}},\ Q_{\text{water}} = Q_{\text{total}},\ Q_{\text{oil}} = 0.0, \tag{A2}$$

(2) *Fluid configuration B.*

In this fluid configuration, oil enters the unit cell from the pore center as seen in Fig. 17(a). Its equivalent electrical diagram is shown in Fig. 17(b), where $W^w_{P\text{-}l}$ is the pore wetting layer resistance and $W^o_{P\text{-}c}$ is the pore oil resistance.

The total equivalent hydraulic resistance of this fluid configuration is given in Eq. (A3), where the notation "//" means that the two resistors are in parallel where $a//b = 1/(1/a+1/b)$. The equivalent water and oil resistances are

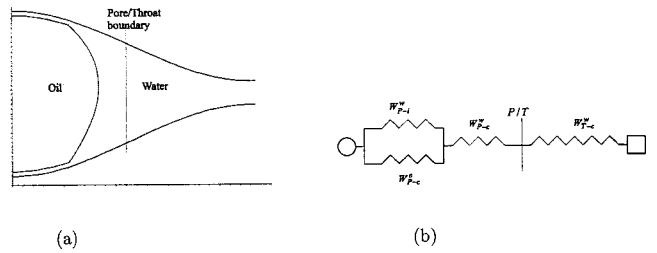

FIG. 17. (a) Fluid configuration B: one oil/water interface (in the pore). (b) The equivalent electrical resistors diagram.

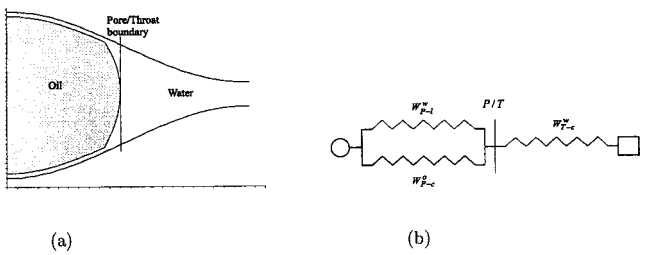

FIG. 18. (a) Fluid configuration C: one oil/water interface (at the pore/throat boundary). (b) The equivalent electrical resistors diagram.

given in Eq. (A4) and (A5) represents the total flow rate, water flow rate, and oil flow rate,

$$W_{\text{eq}} = (W^w_{P\text{-}l} // W^o_{P\text{-}c}) + W^w_{P\text{-}c} + W^w_{T\text{-}c}, \tag{A3}$$

$$W^w_{\text{eq}} = W^w_{P\text{-}l} + W^w_{P\text{-}c} + W^w_{T\text{-}c}, W^o_{\text{eq}} = W^o_{P\text{-}c}, \tag{A4}$$

$$Q_{\text{total}} = \frac{P_P - P_T + P_C}{W_{\text{eq}}}, Q_{\text{water}} = Q_{\text{total}}, Q_{\text{oil}} = 0.0. \tag{A5}$$

(3) *Fluid configuration C.*

This fluid configuration shows oil in the pore branch and water in the throat side [Fig. 18(a)]. Its equivalent electrical diagram is shown in Fig. 18(b).

The total equivalent hydraulic resistance, water equivalent hydraulic resistance, and oil equivalent hydraulic resistance of this fluid configuration is given through Eq. (A6). The total flow rate and the water flow rate is shown through Eq. (A7) while the oil flow rate is given in Eq. (A8):

$$W_{\text{eq}} = (W^w_{P\text{-}l} // W^o_{P\text{-}c}) + W^w_{T\text{-}c}, W^w_{\text{eq}} = W^w_{P\text{-}l} + W^w_{T\text{-}c}, W^o_{\text{eq}} = W^o_{P\text{-}c}, \tag{A6}$$

$$Q_{\text{total}} = \frac{P_P - P_T + P_C}{W_{\text{eq}}},$$

$$Q_{\text{water}} = \left(\frac{P_P - P_T + P_C}{W^w_{P\text{-}l}}\right)\left(1 - \frac{W^w_{T\text{-}c}}{W_{\text{eq}}}\right) \tag{A7}$$

$$Q_{\text{oil}} = Q_{\text{total}} - Q_{\text{water}}. \tag{A8}$$

(4) *Fluid configuration D.*

In this fluid configuration, oil filled the center of the pore and enter the throat as shown in Fig. 19(a). Its equivalent

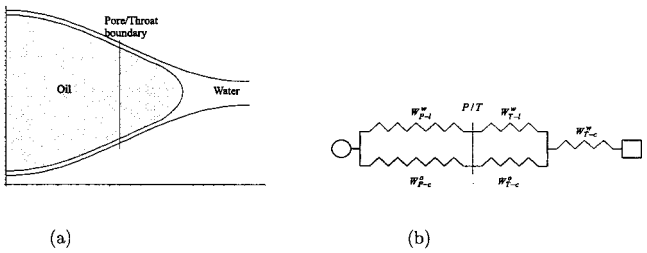

FIG. 19. (a) Fluid configuration D: one oil/water interface (in the throat). (b) The equivalent electrical resistors diagram.

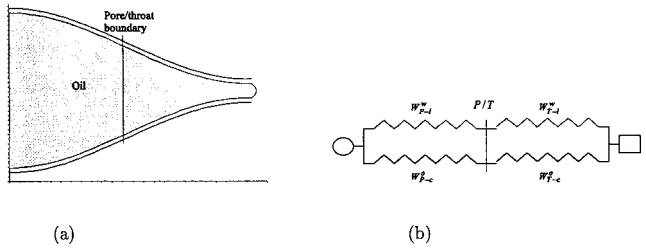

FIG. 20. (a) Fluid configuration E: water in the corners, oil in the center. (b) The equivalent electrical resistors diagram.

electrical diagram is shown in Fig. 19(b), where $W^w_{T\text{-}l}$ is the throat wetting layer resistance and $W^o_{T\text{-}c}$ is the throat oil resistance. The total equivalent hydraulic resistance of this fluid configuration is given in Eq. (A9) and the equivalent water and oil resistances are given in Eq. (A10). The total flow rate is given in Eq. (A11) while Eq. (A12) represents water and oil flow rates:

$$W_{\text{eq}} = [(W^w_{P\text{-}l} + W^w_{T\text{-}l}) // (W^o_{P\text{-}c} + W^o_{T\text{-}c})] + W^w_{T\text{-}c}, \tag{A9}$$

$$W^w_{\text{eq}} = W^w_{P\text{-}l} + W^w_{T\text{-}l} + W^w_{T\text{-}c}, W^o_{\text{eq}} = W^o_{P\text{-}c} + W^o_{T\text{-}c} \tag{A10}$$

$$Q_{\text{total}} = \frac{P_P - P_T + P_C}{W_{\text{eq}}}, \tag{A11}$$

$$Q_{\text{water}} = Q_{\text{total}}\left(\frac{[(W^w_{P\text{-}l} + W^w_{T\text{-}l}) // (W^o_{P\text{-}c} + W^o_{T\text{-}c})]}{W^w_{P\text{-}l} + W^w_{T\text{-}l}}\right),$$

$$Q_{\text{oil}} = Q_{\text{total}} - Q_{\text{water}}. \tag{A12}$$

(5) *Fluid configuration E.*

In this fluid configuration, oil filled the center of pore branch and throat side and the water is only in wetting layers [Fig 20(a)]. Its equivalent electrical diagram is shown in Fig. 20(b).

The total equivalent hydraulic resistance, water equivalent hydraulic resistance, and oil equivalent hydraulic resistance of this fluid configuration is given through Eq. (A13), while Eq. (A14) represents the total flow rate, water flow rate, and oil flow rate:

$$W_{\text{eq}} = (W^w_{P\text{-}l} + W^w_{T\text{-}l}) // (W^o_{P\text{-}c} + W^o_{T\text{-}c}), W^w_{\text{eq}} = W^w_{P\text{-}l} + W^w_{T\text{-}l},$$
$$W^o_{\text{eq}} = W^o_{P\text{-}c} + W^o_{T\text{-}c} \tag{A13}$$

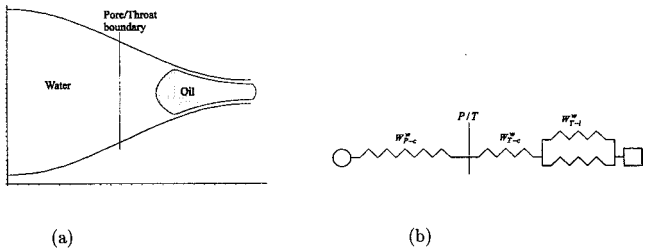

FIG. 21. (a) Fluid configuration F: one oil/water interface (in the throat). (b) The equivalent electrical resistors diagram.

$$Q_{\text{total}} = \frac{P_P - P_T + P_C}{W_{\text{eq}}}, Q_{\text{water}} = \frac{P_P - P_T + P_C}{W_{\text{eq}}^w},$$
$$Q_{\text{oil}} = Q_{\text{total}} - Q_{\text{water}}. \quad \text{(A14)}$$

(6) *Fluid configuration F.*

In this fluid configuration, oil enters the unit cell from the throat center as seen in Fig. 21(a). Its equivalent electrical diagram is shown in Fig. 21(b).

The total equivalent hydraulic resistance, water equivalent hydraulic resistance, and oil equivalent hydraulic resistance of this fluid configuration is given through Eq. (A15), while Eq. (A16) represents the total flow rate, water flow rate, and oil flow rate:

$$W_{\text{eq}} = W_{P\text{-}c}^w + W_{T\text{-}c}^w + (W_{T\text{-}l}^w // W_{T\text{-}c}^o),$$
$$W_{\text{eq}}^w = W_{P\text{-}c}^w + W_{T\text{-}c}^w + W_{T\text{-}l}^w, W_{\text{eq}}^o = W_{T\text{-}c}^o, \quad \text{(A15)}$$

$$Q_{\text{total}} = \frac{P_P - P_T + P_C}{W_{\text{eq}}}, Q_{\text{water}} = Q_{\text{total}}, Q_{\text{oil}} = 0.0. \quad \text{(A16)}$$

[1] P.-E. Øren, S. Bakke, and O.J. Avntzen, Soc. Pet. Eng. J. **3**, 324 (1998).
[2] F.A.L. Dullien, *Fluid Transport and Pore Structure* (Academic Press, San Diego, 1992), 2nd ed.
[3] M.J. Blunt, Curr. Opin. Colloid Interface Sci. **6**, 197 (2001).
[4] M.J. Blunt, M.D. Jackson, M. Piri, and P.H. Valvatne, Adv. Water Resour. **25**, 1069 (2002).
[5] M.J. Blunt, J. Pet. Sci. Eng. **20**, 117 (1998).
[6] P.C. Reeves and M.A. Celia, Water Resour. Res. **32**, 2345 (1996).
[7] H. Hui and M.J. Blunt, J. Phys. Chem. B **104**, 3833 (2000).
[8] A.R. Kovscek, H.Wong, and C.J. Radke, AIChE J. **39**, 1072 (1993).
[9] H.N. Man and X.D. Jing, J. Pet. Sci. Eng. **24**, 255 (1999).
[10] T. Patzek, Soc. Pet. Eng. J. **6**, 144 (2001).
[11] H. Man and X. Jing, Transp. Porous Media **41**, 263 (2000).
[12] D.G. Avraam and A.C. Patayakes, J. Fluid Mech. **293**, 207 (1995).
[13] J. Koplik and T. Lasseter, SPEJ **25**, 89 (1985).
[14] E. Toubou, R. Lenormand, and C. Zarcone, *Immiscible Displacements in Porous Media: Testing Network Simulators by Micromodel Experiments*, Proceedings of the 62nd Annual Technical Conference and Exhibition of the Society of Petroleum Engineers of AIME, SPE 16954, Dallas, TX (1987).
[15] M. Blunt, M.J. King, and H. Scher, Phys. Rev. A **46**, 7680 (1992).
[16] O. Vizika, D.G. Avraam, and A.C. Payatakes, J. Colloid Interface Sci. **165**, 386 (1994).
[17] C.D. Tsakiroglou and A.C. Payatakes, Adv. Colloid Interface Sci. **75**, 215 (1998).
[18] M.S. Valavanides, G.N. Constantinides, and A.C. Payatakes, Transp. Porous Media **30**, 267 (1998).
[19] G.N. Constantinides and A.C. Payatakes, Transp. Porous Media **38**, 291 (2000).
[20] M.S. Valavanides and A.C. Payatakes, Adv. Water Resour. **24**, 385 (2001).
[21] H. Rajaram, L.A. Ferrand, and M.A. Celia, Water Resour. Res. **33**, 43 (1997).
[22] H.K. Dahle and M.A. Celia, Comput. Geosci. **3**, 1 (1999).
[23] R.J. Held and M.A. Celia, Adv. Water Resour. **24**, 325 (2001).
[24] H.F. Nordhaug, M. Celia, and H.K. Dahle, Adv. Water Resour. **26**, 1061 (2003).
[25] E. Aker, K.J. Maløy, A. Hansen, and G.G. Batrouni, Transp. Porous Media **32**, 163 (1998).
[26] H.A. Knudsen, E. Aker, and A. Hansen, Transp. Porous Media **47**, 99 (2001).
[27] H.A. Knudsen and A. Hansen, Phys. Rev. E **65**, 056310 (2002).
[28] M. Blunt and H. Scher, Phys. Rev. E **52**, 6387 (1995).
[29] R. Hughes and M. Blunt, Transp. Porous Media **40**, 295 (2000).
[30] K. Mogensen and E. Stenby, Transp. Porous Media **32**, 299 (1998).
[31] M. Singh and K.K. Mohanty, Chem. Eng. Sci. **58**, 1 (2003).
[32] G. Mason and N.R. Morrow, J. Colloid Interface Sci. **141**, 262 (1991).
[33] D. Zhou, M.J. Blunt, and F.M. Orr, J. Colloid Interface Sci. **187**, 11 (1997).
[34] P.G. Toledo, L.E. Scrlven, and H.T.Davis, *Pore-space Statistics and Capillary Pressure Curves from Volume-controlled Porosimetry*, Proceedings of 64th Annual Technical Conference and Exhibition of the Society of Petroleum Engineers, SPE 19618, San Antonio, TX (1994).